Fabrication of Semiconductor Nanoparticles in a Three-Dimensional Organic-Layered Solid Crystal

Wei Wang,† Xiao Chen,‡ and Shlomo Efrima*

Department of Chemistry, Ben-Gurion University of the Negev, Beer-Sheva 84105, Israel

Received February 4, 1999. Revised Manuscript Received March 30, 1999

We study the in situ fabrication of copper sulfide nanoparticles within a three-dimensional (3D) organic-layered solid crystal of alkylammonium−metal complexes by their reaction with H_2S gas. UV−vis spectroscopy and high-resolution electron microscopy are used to monitor the formation of the nanoparticles and to characterize them. The overall two-dimensional-layered structure of the alkylammonium is preserved during the reaction as seen by FTIR, though deformations near the particles are expected. The reaction kinetics for different chain lengths and metal ions (Cu, Mn, and Cd) have been measured and discussed in terms of the rigidity of the layered 3D structures.

Introduction

Nanoparticles involve unique mesoscopic physics and chemistry and are important also as potential building blocks of higher-order architectures in a wide range of systems and applications.[1−7] Chemists are contributing increasingly to the synthesis and characterization of advanced materials with desired mechanical, optical, electro-optical, magnetic, and electromagnetic properties.[8] Recent colloid chemical approaches have been particularly successful in the preparation of metallic, semiconducting, and magnetic nanoparticles and nanoparticulate films. Current challenges in the production of small inorganic particles is to attain control over their size and shape and to arrange them in ordered or structured systems. To achieve this aim, in situ generation of nanoparticles within or at the interfaces of templates composed of structured surfactant assemblies, micelles, microemulsions, surfactant vesicles, Langmuir monolayers, and Langmuir−Blodgett (LB) films is at present under vigorous investigation.[3,9−11]

In addition, there are recent attempts to generate unique and novel hybrid nanocomposite systems based on inorganic−organic interactions.[12−17] Some of the inspiration (and motivation) for this approach is derived from biological systems in which there is an intimate association between ordered organic self-assembly and the deposition of inorganic materials.[18] Targeting of prefabricated nanoparticles into structured surfactant systems has also been advanced.[19,20]

A novel and interesting approach involves the intercalation of guest inorganic species into organic-layered solids as a way to construct inorganic−organic supramolecular intercalates.[21,22] In comparison to the inclusion of guest species into zeolites[23,24] or clays,[25] intercalation into organic-layered solids is marked by the expandability of their interlayer spaces, and the relative ease of introducing into them specific functionalities. Thus, they can accommodate a wide variety of guest species. Compared to the LB technique, using three-dimensional- (3D-) layered crystals offers the advantage of obtaining macroscopic systems, yet retaining the microscopic two-dimensional (2D) anisotropy.

* To whom correspondence should be addressed.
† Current address: Department of Chemistry, University of Pittsburgh, Pittsburgh, PA 15260.
‡ Permanent address: Institute of Colloid and Interface Chemistry, Shandong University, Jinan, Shandong 250100, People's Republic of China.

(1) Herron, N.; Thorn, D. L. *Adv. Mater.* **1998**, *10*, 1173.
(2) Alivisatos, A. P. *J. Phys. Chem.* **1996**, *100*, 13226.
(3) (a) Fendler, J. H.; Meldrum, F. C. *Adv. Mater.* **1995**, *7*, 607. (b) Fendler, J. H. In *Nanoparticles and Nanostructured Films*; Fendler, J. H., Eds.; Wiley-VCH: Weinheim, 1998; pp 429−461. (c) Meldrum, F. C.; Fendler, J. H. In *Biomimetic Materials Chemistry*; Mann, S., Eds.; VCH: New York, 1996; pp 175−219.
(4) Murray, C. B.; Kagan, C. R.; Bawendi, M. G. *Science* **1995**, *270*, 1335.
(5) Weller, H. *Angew. Chem., Int. Ed. Engl.* **1993**, *32*, 41.
(6) Rosencher, E.; Fiore, A.; Vinter, B.; Berger, B.; Bois, P.; Nagle, J. *Science* **1996**, *271*, 168.
(7) Ramsay, J. D. F. *Curr. Opin. Colloid Interface Sci.* **1996**, *1*, 208.
(8) Ozin, G. A. *Adv. Mater.* **1992**, *4*, 612.
(9) Belloni, J. *Curr. Opin. Colloid Interface Sci.* **1996**, *1*, 184.
(10) Pileni, M. P. *J. Phys. Chem.* **1993**, *97*, 6961.
(11) Brus, L. *Curr. Opin. Colloid Interface Sci.* **1996**, *1*, 197.
(12) (a) Mayya, K. S.; Sastry, M. *Langmuir* **1997**, *13*, 2575. (b) Mayya, K. S.; Sastry, M. *Langmuir* **1998**, *14*, 74.
(13) (a) Guo, S.; Popovitz-Biro, R.; Weissbuch, I.; Cohen, H.; Hodes, G.; Lahav, M. *Adv. Mater.* **1998**, *10*, 121. (b) Guo, S.; Popovitz-Biro, R.; Arad, T.; Hodes, G.; Leiserowitz, L.; Lahav, M. *Adv. Mater.* **1998**, *10*, 657.
(14) (a) Ogawa, M.; Kuroda, K. *Bull. Chem. Soc. Jpn.* **1997**, *70*, 2593. (b) Ogawa, M.; Igarashi, T.; Kuroda, K. *Bull. Chem. Soc. Jpn.* **1997**, *70*, 2833.
(15) Kimizuka, N.; Kunitake, T. *Adv. Mater.* **1996**, *8*, 89.
(16) Cao, G.; Lynch, V. M.; Yacullo, L. N. *Chem. Mater.* **1993**, *5*, 1006.
(17) Talham, D. R.; Seip, C. T.; Whipps, S.; Fanucci, G. E.; Petruska, M. A.; Byrd, H. *Comments Inorg. Chem.* **1997**, *19*, 133.
(18) (a) Mann, S. *Nature* **1993**, *365*, 499. (b) Mann, S. In *Biomimetic Materials Chemistry*; Mann, S., Eds.; VCH: New York, 1996; pp 1−10.
(19) (a) Fabre, P.; Casagrande, C.; Veyssie, M.; Cabuil, V.; Massart, R. *Phys. Rev. Lett.* **1990**, *64*, 539. (b) Quilliet, C.; Fabre, P.; Cabuil, V. *J. Phys. Chem.* **1993**, *97*, 287. (c) Ramos, L.; Fabre, P.; Dubois, E. *J. Phys. Chem.* **1996**, *100*, 4533. (d) Ponsinet, V.; Fabre, P. *J. Phys. Chem.* **1996**, *100*, 5035.
(20) (a) Quilliet, C.; Ponsinet, V.; Cabuil, V. *J. Phys. Chem.* **1994**, *98*, 3566. (b) Ramos, L.; Fabre, P.; Ober, R. *Eur. Phys. J. B* **1998**, *1*, 319.
(21) Ogawa, M.; Kuroda, K. *Chem. Rev.* **1995**, *95*, 399.
(22) Schollhorn, R. *Chem. Mater.* **1996**, *8*, 1747.
(23) Stucky, G. D. *Prog. Inorg. Chem.* **1992**, *40*, 99.
(24) Wang, Y.; Herron, N. *J. Phys. Chem.* **1987**, *91*, 257.
(25) Michalik, J.; Yamada, H.; Brown, D. R.; Kevan, L. *J. Phys. Chem.* **1996**, *100*, 4213.

10.1021/cm990079a CCC: $18.00
Published on Web 06/10/1999

In a pioneering work, Lahav et al. have successfully prepared semiconductor nanoparticles in situ within layered organic matrixes by a gas−solid reaction.[13] Cao et al. also briefly mentioned the possibility to form sulfide particles directly in metal organophosphonates layered solids.[16]

In this report, we extend the work of Lahav et al.[13] to other systems and expand on it. We choose 3D lamellar crystals of tetrahalos of bis(*n*-alkylammonium). We focus on $(C_nH_{2n+1}NH_3)_2CuCl_4$, with $n = 10$, 12, 14, 16, and 18. However, also the Mn and Cd analogous systems are prepared. These compounds are known to crystallize in a 2D perovskite-type structure and exhibit interesting magnetic and structural properties.[26−29] Within the crystal, the nearly separate inorganic MCl_4^{2-} ($M = Cu$, Mn, and Cd) sheets are sandwiched between two hydrocarbon layers and the separation of these sheets is determined by the width of the alkylammonium bilayer. We show here that these layered compounds provide appropriate matrixes for the preparation of nanoparticles of chalcogenides by in situ reaction with H_2S. We also discuss the rates of formation of the particles and show that they are strongly dependent on the length of the hydrocarbon chain.

Experimental Section

Materials. Decylamine (95%), dodecylamine (≥98%, GC), hexadecylamine (99%), copper(II) chloride (97%), and cadmium chloride (99%) are purchased from Aldrich. Tetradecylamine (>99%, GC), octadecylamine (>99%, GC), hydrochloric acid (32%), and sulfuric acid (>97.5%) are from Fluka. Manganese(II) chloride tetrahydrate (GR, ACS) and sodium sulfide (GR) are Merck products. Ethyl alcohol (≥99.8%, analytical) was provided by Frutarom. All the chemicals are used as received. Water is of ∼18 MΩ cm resistivity, obtained from a Barnstead E-pure water purifier.

2. Synthesis. The samples of *n*-alkylammonium chlorides (C_nCl, where *n* is the number of carbon atoms, $n = 10$, 12, 14, 16, and 18) are prepared from their corresponding *n*-alkylamines, according to previously described procedures.[30] Bis(*n*-alkylammonium) tetrachlorocuprates (C_nCuCl) are synthesized by the reaction of C_nCl with stoichiometric amounts of the corresponding $CuCl_2$ in an absolute ethanol solution.[31] The mixture is refluxed for 30 min, the solvent evaporated, and the solid crystallized repeatedly three times from ethanol. Gold yellow C_nCuCl lamellar crystals are obtained. The analogue (pale pink) Mn and (white) Cd crystals are produced in a similar fashion starting from the appropriate chlorides. Their sulfides are produced by exposing the corresponding crystals to H_2S gas at room temperature under atmospheric pressure. H_2S gas is prepared by reacting Na_2S with dilute H_2SO_4.

3. Measurements. Infrared spectra are recorded with 4 cm^{-1} resolution using a Nicolet Impact 410 FTIR spectrometer. Thin crystalline films of the samples are deposited on KCl windows from their absolute ethanol solutions.

UV−visible absorption spectra are measured by a HP-8452A diode array spectrophotometer with a resolution of 2 nm and a 0.5 s exposure time. Thin films of the alkylammonium cuperates are deposited onto quartz windows or glass slides from an absolute ethanol solution by spin casting at a speed of 650−900 rpm at room temperature. The film thickness is estimated to be several hundred nanometers, on the basis of the concentration of the spreading solution and its density and amount. Then, the films are subjected to H_2S gas.

The sulfide particles that form are observed by transmission electron microscopy (TEM) in a JEOL 1200 EXII electron microscope using an acceleration voltage of 100 kV. A drop of the absolute ethanol solution of C_nCuCl is placed on a holey carbon film supported by a 300 mesh copper grid (TED PELLA, Inc. catalogue no. 01883-F). On the basis of volume of the drop placed on the grid, about half of which is wiped away, the thickness of the crystal film is estimated to be about 20−40 nm. After the evaporation of the solvent, the sample-covered grid is exposed to H_2S gas to form the sulfide. The size distribution of the sulfide particles is obtained by digitizing the micrographs and analyzing 500 particles using the public domain NIH Image 2.0 software developed at the U.S. National Institute of Health.

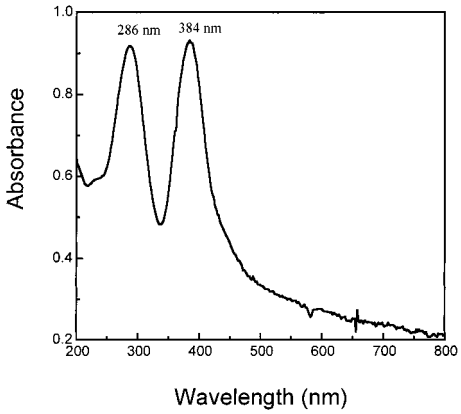

Figure 1. UV−visible absorption spectrum of a $C_{10}CuCl$ thin film.

Results and Discussion

1. UV−Visible Absorption Spectroscopy. Thin films of crystalline C_nCuCl exhibit two distinct exciton absorption bands at 286 and 384 nm (Figure 1).[15,32] The absorption features are practically independent of the length of *n*-alkylammonium chains and are not observed for the C_nCl crystal in the absence of Cu^{2+} ions. Reaction with H_2S gas causes a gradual disappearance of these bands. After completion of the reaction, the UV−vis absorption spectra lose all distinct features in the near UV and visible region, exhibiting only monotonically increasing extinction in the UV side (Figure 2), similar to that of a copper sulfide particulate film.[33] The absorption onset is located at ∼700 nm. As the spectra are very broad and featureless, it is impossible to discern any differences in the onset for the C_{10}, C_{12}, and C_{18} chains. FTIR shows that there are not any significant changes on the alkylamine region (see section 3). This means that the general structure is conserved, only the $CuCl_4^{2-}$ is replaced.

The mineralogy of the Cu−S system is complex and demonstrates many stable phases with the stoichiometry ranging between that of chalcocite (Cu_2S) and covellite (CuS),[34] each with its specific optical properties.

(26) Bellitto, C.; Day, P. *Compre. Supramol. Chem.* **1996**, *7*, 293.
(27) (a) Kind, R.; Plesko, S.; Arend, H.; Blinc, R.; Zeks, B.; Seliger, J.; Lozar, R.; Slale, J.; Levstik, A.; Filipic, C.; Zagar, V.; Lahajnar, G.; Milia, F.; Chapuis, G. *J. Chem. Phys.* **1979**, *71*, 2118. (b) Kind, R.; Blinc, R.; Arend, H.; Muralt, P.; Slak, J.; Chapuis, G.; Schenk, K. J.; Zeks, B. *Phys. Rev. A* **1982**, *26*, 1816.
(28) Blinc, R.; Burgar, M. I.; Rutar, V.; Zeks, B.; Kind, R.; Arend, H.; Chapuis, G. *Phys. Rev. Lett.* **1979**, *43*, 1679.
(29) Busico, V.; Cernicchiaro, P.; Corradini, P.; Vacatello, M. *J. Phys. Chem.* **1983**, *87*, 1631.
(30) Wang, W.; Li, L. M.; Xi, S. Q. *J. Phys. Chem. Solids* **1993**, *54*, 73.
(31) Guo, N.; Wang, W. *Chin. J. Chem. Phys.* **1995**, *8*, 53.
(32) Calabress, J.; Jones, N. L.; Harlow, R. L.; Herron, N.; Thorn, D. L.; Wang, Y. *J. Am. Chem. Soc.* **1991**, *113*, 2328.
(33) Nair, M. T. S.; Nair, P. K. *Semicond. Sci. Technol.* **1989**, *4*, 191.

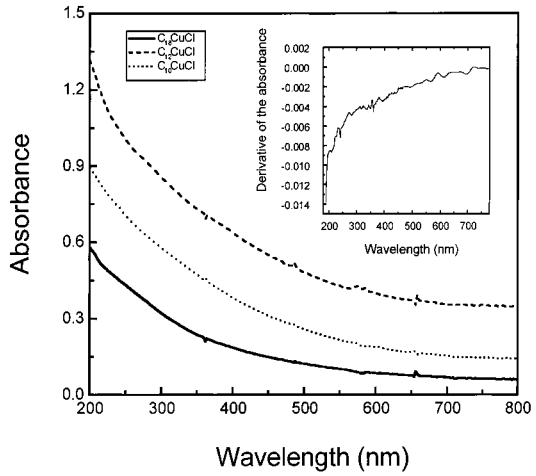

Figure 2. UV−visible absorption spectra of C_nCuCl after reaction with H_2S. $n = 10$, 12, and 18. The inset is the first-derivative spectrum for $C_{10}CuCl$.

CuS gives a characteristic broad absorption band in the near-IR region (~920 nm)[35] which decreases on increasing the sulfur content, leading to the appearance of an apparent edge onset at a shorter wavelength (from 550 to 830 nm).[36] Cu_2S, in contrast, is an opaque and dark crystal which adsorbs over the entire visible region with an onset at 1022 nm.[37] Comparing the absorption onsets in Figure 2 (~700 nm) with those reported by Engelken et al.,[36] we tentatively assign the spectra to copper sulfide, Cu_xS, with x between 1.6 and 1.8. The apparent blue-shifted absorption onset (from 1022 to 700 nm), if interpreted as a size quantization effect, suggests the presence of nanoscale particles in the 3D organic crystal. The Mn and Cd compounds yield featureless extinction spectra, increasing monotonically for short wavelengths, both prior to H_2S treatment and after it.

2. TEM of the Cu_xS Product. High-resolution electron microscopy reveals that Cu_xS nanoparticles form. Lahav et al., too, looked at thiol-capped particles in an organic carboxylate crystal.[13a,b] Figure 3 shows TEM pictures of Cu_xS particles formed in situ in the thin $C_{10}CuCl$ film. Many spherical particles can be observed in several regions of the grid (Figure 3A,B). The particles do not originate from the copper grid itself, as they are observed on the carbon film extending across the grid spaces. Energy-dispersive spectrometry (EDS) element microanalysis shows clear existence of sulfur and, of course, copper. Comparing parts A and B of Figure 3, we see that different size distributions are apparent for different regions of the film, though the particle populations are rather uniform at a given site. We take this to reflect the inhomogeneity of the film and its effect on diffusion of the reactants in it. In accordance with that we also see, at times, regions of aggregated particles. They are more prominent for the long-chain alkyls.

Figure 4, parts a−d, shows that particles form also from $C_{12}CuCl$−$C_{18}CuCl$, indicating that the particle

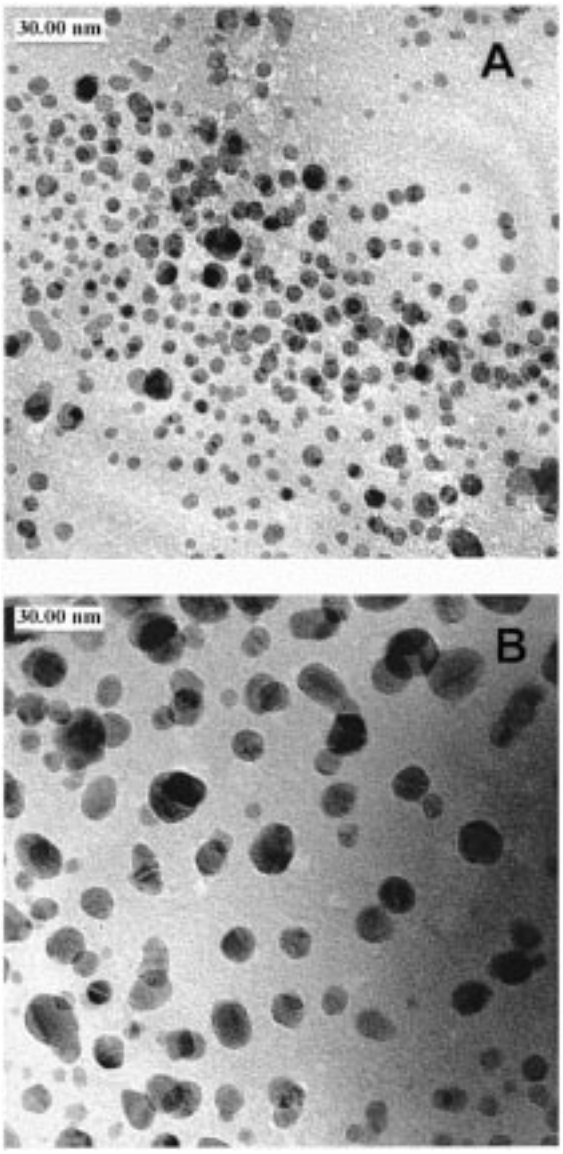

Figure 3. TEM images of the Cu_xS particles formed in a thin film of $C_{10}CuCl$. A and B are at two different regions.

sizes are rather similar. Two typical histograms of the size distribution taken respectively from parts A and B of Figure 3 are shown in Figure 5. The particle mean diameters are 4.6 ± 1.4 nm for region A and 9.2 ± 3.1 nm for region B. This suggests that if one learns to control the homogeneity of the film and the diffusion conditions one can achieve quite monodisperse particles.

Some particles are notably crystalline (Figure 4a, marked by arrows), with well-resolved lattice planes being observed. The interplanar distance is not the same for all the particles, and it ranges from 0.34 to 0.62 nm. This corresponds to the known range of the lattice spacing values for different crystalline faces of chalcocite or covellite.[38]

It should be noted that because of the lack of precise control of the H_2S pressure or the gas flow rate in the reaction vessel during H_2S exposure, as well as the inhomogeneity of the films, it is not presently very meaningful to quantitatively compare the particle sizes

(34) Bailar, J. C., Ed. *Comprehensive Inorganic Chemistry*, 1st ed.; Pergamon Press: Oxford, 1973; Vol. 3.
(35) Silvester, E. j.; Grieser, F.; Sexton, B. A.; Healy, T. W. *Langmuir* **1991**, *7*, 2917.
(36) Engelken, R. D.; McCloud, H. E. *J. Electrochem. Soc.* **1985**, *132*, 567.
(37) Marshall, R.; Mitra, S. S. *J. Appl. Phys.* **1965**, *36*, 3882.
(38) Powder Diffraction File (PDF) No. 33-490 and 6-464 of International Center for Diffraction Data (ICDD), Joint Committee on Powder Diffraction Standards (JCPDS): Pennsylvania, 1984.

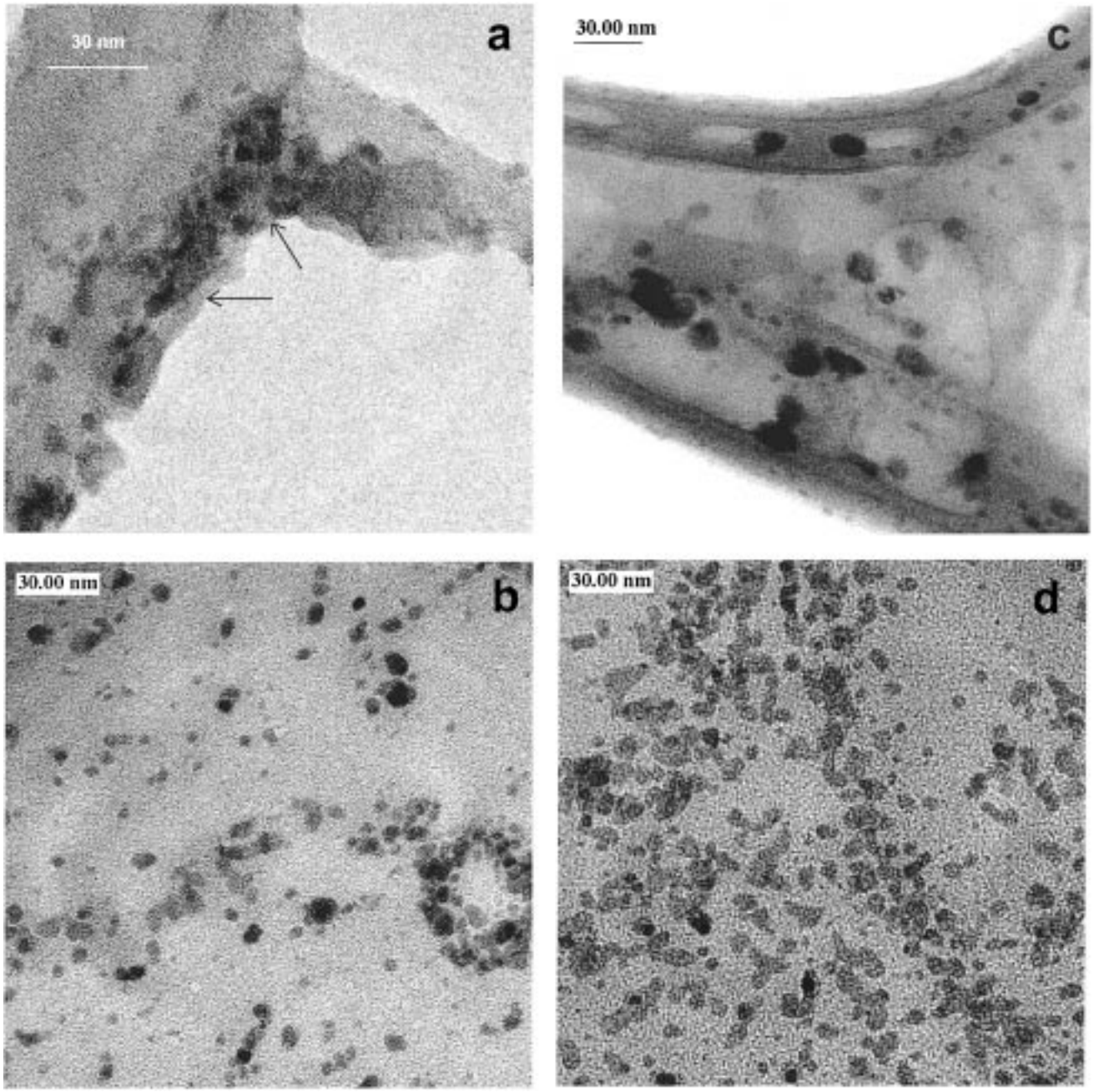

Figure 4. TEM images of the Cu_xS nanoparticles in (a) $C_{12}CuCl$; (b) $C_{14}CuCl$; (c) $C_{16}CuCl$; (d) $C_{18}CuCl$. The arrows in (a) point to apparently crystalline particles.

produced for the different alkyl chain-length samples. However, the basically similar appearance of the particles, and the use of similar experimental conditions for all samples (except exposure time), shows that there is no apparent dependence of the size of the Cu_xS particles formed in the various films.

We have not studied yet the Mn and Cd compounds by TEM, the focus of this report being on copper.

3. FT-IR Transmission Spectroscopy. To investigate the effect of the formation of the chalcogenide particles on the crystal structure of the host, a series of FTIR spectra are compared. Consider, for example, the $C_{10}CuCl$ system. The IR spectra of $C_{10}CuCl$, the product produced by reacting it with H_2S, and $C_{10}Cl$ are shown in Figure 6. Overall, the spectra for $C_{10}Cl$ and the product after treatment with H_2S are practically identical, while that of $C_{10}CuCl$ is significantly different.

The C−H stretches are found in the region between 3000 and 2800 cm^{-1}, and their positions reflect the extent of organization in the alkyl chains. More specifically, the frequency of the methylene stretch is sensitive to conformation.[39,40] The peak positions of the two characteristic CH_2 stretches for $C_{10}CuCl$ appear at 2920 ($\nu^{as}_{CH_2}$) and 2850 cm^{-1} ($\nu^{s}_{CH_2}$), respectively (Figure 6a). The peak position of $\nu^{as}_{CH_2}$ indicates that at least part of the alkyl chain segments are in a close-packing arrangement with an all-trans conformation.[41,42]

(39) Maoz, R.; Sagiv, J. *J. Colloid Interface Sci.* **1984**, *100*, 465.
(40) Porter, M. D.; Bright, T. B.; Allara, D. L.; Chidsey, C. E. D. *J. Am. Chem. Soc.* **1987**, *109*, 3559.
(41) Tillman, N.; Ulman, A.; Schildkraut, J. S.; Penner, T. L. *J. Am. Chem. Soc.* **1988**, *110*, 6136.
(42) Hostetler, M. J.; Stokes, J. J.; Murray, R. W. *Langmuir* **1996**, *12*, 3604.

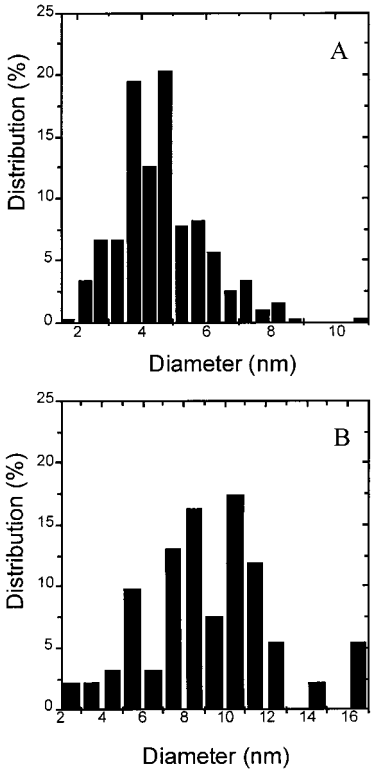

Figure 5. Histograms of the size distribution of Cu_xS particles generated in a $C_{10}CuCl$ film taken respectively from parts A and B of Figure 3.

After reaction with H_2S, these C−H vibrational modes move slightly to 2916 and 2848 cm^{-1} and coincide with those observed in $C_{10}Cl$ (Figure 6b,c). Thus, the formation of Cu_xS reverts the structure back to that of the crystal devoid of copper ions, maintaining the layered solid structure. The Cu_xS particles do not disturb this structure significantly. This is plausible as the number density of the particles is very low.

The CH_2 scissoring modes in $C_{10}CuCl$ are manifested in two peaks at 1470 and 1479 cm^{-1}, which are known to arise from the crystal field effects.[43] Such splitting is also observed for the CH_2 wagging mode at 721 and 727 cm^{-1}. Reaction with H_2S reduces the crystal field effects. Only single bands at 1468 and 721 cm^{-1} for these vibration modes are seen, which is similar to $C_{10}Cl$. In the spectral region 1200−1350 cm^{-1} other differences are seen for the film, before and after reaction with H_2S (Figure 7). These features are the twisting and rocking progression bands. Their presence is an indicator of crystallinity and an all-trans packing of the alkyl chains.[42,44]

IR spectroscopy can also be used to compare the nature of copper ion−NH_3 binding before and after the reaction. It is known that the cavities between the $CuCl_6$ octahedra are occupied by the $-NH_3^+$ polar heads of the *n*-alkylammonium groups which are involved in N−H···Cl hydrogen bonds.[27,28] In addition, van der Waals interactions between the alkyl chains and Coulomb forces between the positively charged organic ions and the negatively charged inorganic metallic sheets account for the interlayer bonding.[45] Consequently, the vibrations related to the NH_3 groups are sensitive to structural changes of the inorganic sheets in the crystals.[30,31,46,47] The N−H stretching vibrations of $C_{10}CuCl$

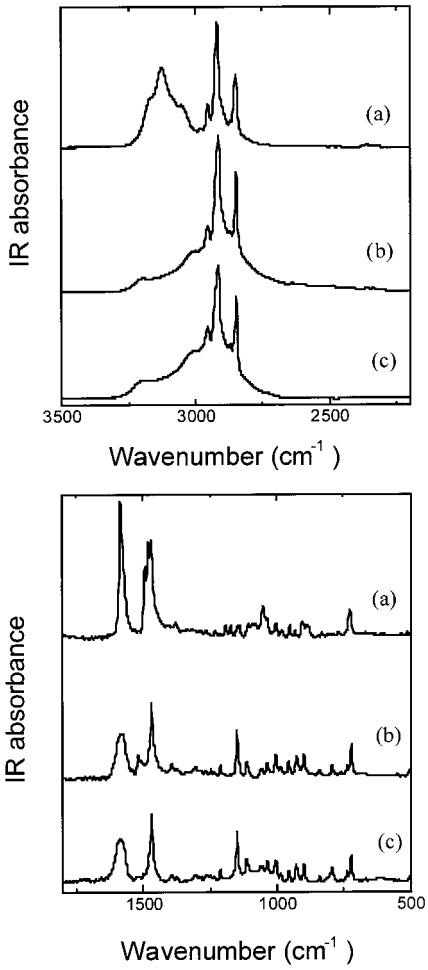

Figure 6. FTIR spectra (a) of a crystallized $C_{10}CuCl$ thin film, (b) after completion of the reaction of $C_{10}CuCl$ thin films with H_2S gas, and (c) of a crystallized $C_{10}Cl$ thin film.

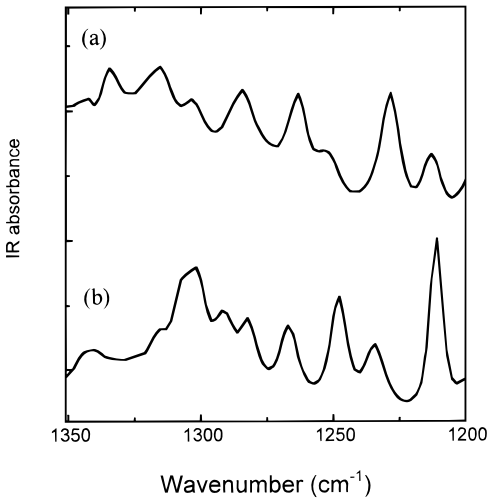

Figure 7. Twisting and rocking progression bands in the FTIR spectra of $C_{10}CuCl$ before (a) and after (b) treatment with H_2S.

(43) Rabolt, J. F.; Burns, F. C.; Schlotter, N. E.; Swalen, J. D. *J. Chem. Phys.* **1983**, *78*, 946.
(44) Yang, J.; Peng, X. G.; Zhang, Y.; Wang, H.; Li, T. J. *J. Phys. Chem.* **1993**, *97*, 4484.
(45) Geick, R.; Strobel, K. *J. Phys. C* **1979**, *12*, 27.

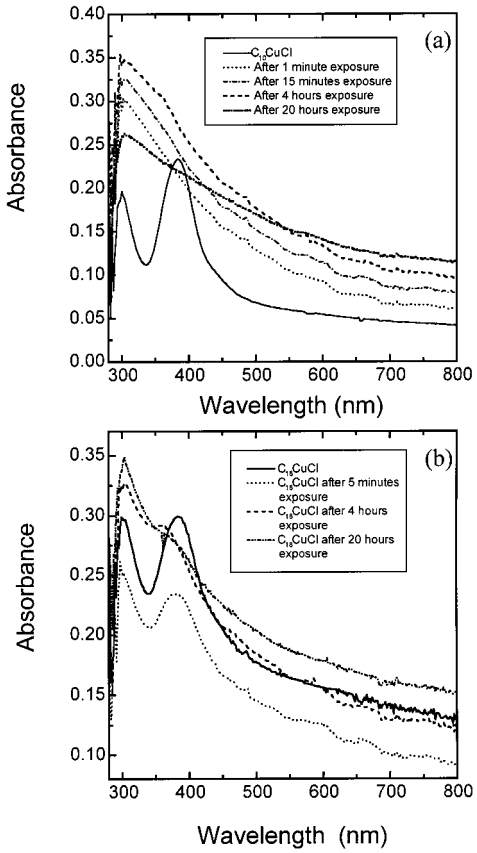

Figure 8. UV−visible spectra for $C_{10}CuCl$ and $C_{18}CuCl$ films at different exposure times to H_2S.

exhibit strong and broadened absorption bands with two peaks at 3126 and 3053 cm^{-1}, with two shoulders at 3166 and 3075 cm^{-1}. They stem from various hydrogen-bonding arrangements of the $RNH_3\cdots Cl$ group. The NH_3 asymmetric and symmetric deformation vibrations appear at 1583 and 1491 cm^{-1} (Figure 6a), respectively. After completion of the reaction of $C_{10}CuCl$ with H_2S, the N−H stretch and deformation bands are much weaker and appear at 3195 and 1580 cm^{-1} (Figure 6b), once again very similar to what is observed in a $C_{10}Cl$ crystal.[30,46] The H_2S treatment practically exhausts the copper ions, eliminating the special arrangement of hydrogen bonding observed in the $C_{10}CuCl$ crystal and reverting back to the $C_{10}Cl$ structure. Similar conclusions are reached for Mn and Cd compounds.

4. Reaction Kinetics of the Particle Formation. The specific microenvironment of the layered metal−organic solid should have an effect on the chemical reactions that take place in it. Specifically, it can affect the reaction rate, as observed here, by channeling the diffusion of the incoming H_2S, the motion of ions along special paths, and the growth of the particles within and beyond the interlayer spacing.

We indeed find that the chain length of the alkylammonium separating the ionic layers within the crystal strongly affects the reaction rate with H_2S. The reaction of the thin film of the crystal with H_2S is over within half an hour for $C_{10}CuCl$, while it takes 4 h for $C_{14}CuCl$ and about 20 h for $C_{18}CuCl$. The kinetics of the gas−solid reaction is monitored by UV−visible spectroscopy measured at different reaction times.

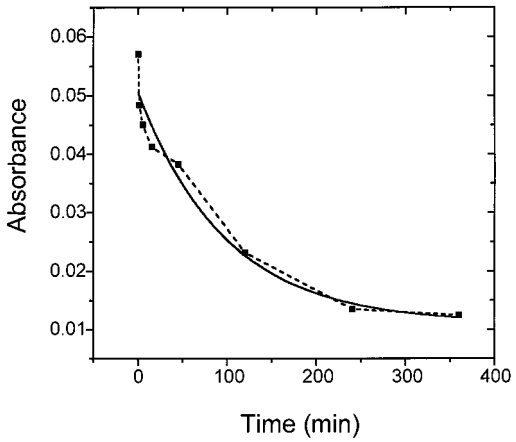

Figure 9. Intensity changes with time of the peak at 384 nm in the UV−visible absorption spectrum of $C_{18}CuCl$ reacting with H_2S (dashed line). The solid curve is an exponential decay best fit. The 384 nm peak was corrected for the steeply rising background.

Figure 8 shows the results for $C_{10}CuCl$ and $C_{18}CuCl$ thin films (denoted henceforth by C10 and C18, respectively), spin cast on glass slides at 650−1000 rpm. Before the reaction, they all show the exciton peak at 384 nm (the 286 nm peak is obscured in the opaque region of the glass). For C18 this peak is broader with a reduced relative height.

Within a single minute of exposure, the 384 nm peak for C10 completely disappears (Figure 8a) and shows little change for further exposure up to 5 min. At 15 min, a shoulder at about 364 nm begins to emerge. In contrast, short exposures of the C18 film lead only to a lowering of the whole spectrum, maintaining its shape. After 15 min the C18 film's spectrum still does not change much (not shown).

Prolonged exposure to H_2S strengthens the shoulder in the spectrum of the C10 film. In parallel, the peak in the C18 film diminishes and finally, after 4 h, reduces to a distinct shoulder on the broad, steeply increasing extinction background (Figure 8b). After 20 h, the shoulder for C10 disappears completely, while it is still discernible for the C18 film.

These observations demonstrate the big difference in the reaction rates for the compounds of different chain lengths. The decrease of the peak at 384 nm can be used as a measure of the progress of the reaction. Figure 9 shows the intensity of the 384 nm absorption peak as a function of the reaction time of a C18 crystal film. The spectra are background-corrected. The decay is exponential with a characteristic time of 98 min (±34 min). This rate is at least 2 orders of magnitude slower than the reaction of the C10 film. Recall that the latter reacts faster than we can measure.

It is plausible that the H_2S penetrates preferentially along the lamellae in the alkylammonium crystal, retaining the full structure of C_nCl as confirmed by FTIR measurements. Similarly, the motion of the copper ions is expected to proceed laterally. The chain length in itself is not expected to affect the inorganic layer distance much (as suggested by the X-ray results of Vacatello et al.[48]). Compounds with longer chains may

(46) Casal, H. L.; Cameron, D. G.; Mantsch, H. H. *J. Phys. Chem.* **1985**, *89*, 5557.
(47) Ricard, L.; Cavagnat, R.; Rey-Lafon, M. *J. Phys. Chem.* **1985**, *89*, 4887.

have more compact and rigid structures which can slow the motion and the necessary dislocation of the copper ions. Barraud et al. suggested that 22-carbon chains showed a greater lateral cohesion than that of 18-carbon chains in carboxylic acid multilayers, implying a more rigid structure.[49] An increase in the thickness of the organic layer for longer-chain compounds and their increasing cohesion are possible reasons for significant retardation of H_2S diffusion along the chain direction, through the layer, and its channeling in the lateral direction. Energy data concerning a conformation transition of the C_nCl chain also support this deduction.[29] Conformational melting in $C_{10}Cl$ occurs at 321 K, but is 65 K higher for $C_{18}Cl$. The ΔH and ΔS for such melting are 4.17 kJ/mol and 13.0 J/K·mol for $C_{10}Cl$ and 7.86 kJ/mol and 20.4 J/K·mol for $C_{18}Cl$. They suggest that the longer chains render the crystal more rigid, decreasing the accessibility of the deformations needed for the formation of the sulfide particles.

Our results also suggest that the slow stage in the entire process is the diffusion of H_2S into the interior of the crystal. This is seen by the fact that the spectra do not change after the samples are removed from the H_2S compartment. This is consistent with a picture of "side-loading" of H_2S, via channeling along the lamellae. Slow diffusion of H_2S along these planes causes accumulation at the entry points at the edges. This prevents additional loading until diffusion and subsequent reaction deplete these regions. Possible evaporation of the small amount of H_2S trapped at the entry region, upon removal of the sample from the treatment cell, is still in agreement with the mechanism above. We do not believe that the motion of Cu ions controls the rate (with the longer-chain compounds), as in that case, we would expect the reaction to continue also outside of the H_2S cell. After all, the Cu ions have an extremely large affinity to S^{2-}, and one expects them to react in whatever complex form they are. Thus, S^{2-} would bond to Cu^{2+} in the chloride complex, just as well as on the surface of a growing copper sulfide particle.

Notwithstanding this, similar measurements for the Mn and Cd C10-chain systems show the rates to be strongly dependent on the nature of the cation. While the reaction for Cu is over in a few minutes, the analogous reaction for Mn takes several hours and for Cd tens of hours are required. For the C18 compounds the rates are tens of hours/2−3 days/3−4 days for Cu/Mn/Cd, respectively. On one hand, this trend could indicate that the interaction between the metal ions and ligands is of paramount importance in determining the overall rate of the reaction. On the other hand, with the different ions the distances within the crystal may be different, or perhaps more importantly, the rigidity may also vary. Both certainly can affect motion along the planes in the crystal, that of H_2S as well as that of the metal ions.

Another major consideration involves the relative size of the emerging copper sulfide particles and the interlayer spacing. The particles eventually reach sizes of 3−6 nm, while the width of the inorganic layer is estimated from the ionic radii of Cl^- and M^{2+} to be 0.43−0.46 nm.[50] Thus, to accommodate the particles, there necessarily should be considerable local distortion of the crystal structure. This calls to mind CdS formed in cadmium arachidate LB films.[51] This requires the alkyl chains to tilt or interdigitate. This might be easier for Cu than for Cd because the chains of the former are all parallel, while those of the latter form a zigzag arrangement parallel to the crystal *c* axis.[52] Both interdigitation and change of tilt are more feasible for parallel chains.

The different structures of the Cu and Cd crystals are also manifested in their different solubilities in alcohol. $C_{10}CdCl$ is much less soluble than the C10 crystals of Cu and Mn. By comparing lattice heat capacity, Bloembergen et al.[53] also indicated that there is a somewhat larger value of the intralayer (and interlayer) couplings for Cd compounds than those of the Cu analogues.

All the considerations given above suggest that the large differences in the H_2S−metal ion reaction kinetics in the layered alkylammonium crystals for different chain lengths and ions is most probably due to the different rigidities of the lattices.

Conclusions

In conclusion, we have taken advantage of the unique 2D-layer arrangement of metal ions within 3D crystals, and the preferential lateral motion of H_2S within them, to construct organic−inorganic hybrid systems. Nanosized semiconductor particles are produced in situ within the 3D crystal matrixes. The generation of the chalcogenide nanoparticles does not influence the overall structure of the organic molecules much in the 2D-layered crystal, though local deformations are unavoidable. Significant effects of the chain length of the organic compounds and the metal ions on the rates are observed and interpreted in terms of the differences in the rigidities of the crystals.

The method presented here has several merits: (1) It substantiates a little studied and effective way to incorporate nanoparticles into structured layer crystals. (2) Powders of the 3D lamellar crystals can serve as templates for producing large quantities of nanoparticles. (3) The reaction conditions are simple and easily controlled.

Acknowledgment. This work was supported by the Israel Science Foundation founded by the Israel Academy of Science and Humanities. Chen also would like to acknowledge the financial support from the Chinese Scholarship Council and State Major Basic Research Project of China for his stay in Israel.

CM990079A

(48) Vacatello, M.; De Girolamo, M.; Busico, V. *J. Chem. Soc., Faraday Trans. 1* **1981**, *77*, 2367.
(49) Barraud, A.; Rosilio, C.; Ruaudel-Teixier, A. *Thin Solid Films* **1980**, *68*, 7.
(50) Weast, R. C., Ed. *CRC Handbook of Chemistry and Physics*, 57th ed.; CRC Press: Cleveland, OH, 1977; p F213.
(51) Dhanabalan, A.; Kudrolli, H.; Major, S. S.; Talwar, S. S. *Solid State Commun.* **1996**, *99*, 859.
(52) Kozelj, M.; Rutar, V.; Zupancic, I.; Blinc, R.; Arend, H.; Kind, R.; Chapuis, G. *J. Chem. Phys.* **1981**, *74*, 4123.
(53) Bloembergen, P.; Miedema, A. R. *Physica* **1974**, *75*, 205.